Materials Science and Engineering C 35 (2014) 85–91

Contents lists available at ScienceDirect

Materials Science and Engineering C

journal homepage: www.elsevier.com/locate/msec

Development of amperometric L-tyrosine sensor based on Fe-doped hydroxyapatite nanoparticles

P. Kanchana, N. Lavanya, C. Sekar *

Department of Bioelectronics and Biosensors, Alagappa University, Karaikudi-630003, Tamil Nadu, India

ARTICLE INFO

Article history:
Received 30 May 2013
Received in revised form 18 September 2013
Accepted 19 October 2013
Available online 1 November 2013

Keywords:
L-tyrosine
tyrosinase
Fe-doped hydroxyapatite
direct electrochemistry
biosensor

ABSTRACT

A novel biosensor based on Fe-doped hydroxyapatite (Fe-HA) nanoparticles and tyrosinase has been developed for the detection of L-tyrosine. Nanostructured Fe-HA was synthesized by a simple microwave irradiation method, and its phase formation, morphology and magnetic property were examined by powder X-ray diffraction (XRD), transmission electron microscopy (TEM) and vibrating sample magnetometer (VSM). Electrochemical performance of the nano Fe-HA/tyrosinase modified glassy carbon electrode (GCE) for detection of L-tyrosine was investigated by cyclic voltammetry (CV) and amperometric methods. The fabricated biosensor exhibited a linear response to L-tyrosine over a wide concentration range of 1.0×10^{-7} to 1.0×10^{-5} M with a detection limit of 245 nM at pH 7.0. In addition, the fabricated sensor showed an excellent selectivity, good reproducibility, long-term stability and anti-interference towards the determination of L-tyrosine.

1. Introduction

Hydroxyapatite [$Ca_{10}(PO_4)_6(OH)_2$], a main inorganic component of bone, has been extensively applied in biomedical implants, bone regeneration, drug delivery, protein separation and immunosensors owing to its excellent biocompatibility, bioactivity and multi-adsorbing sites [1]. Due to the excellent biocompatibility and adsorbability, nanostructured hydroxyapatite (HA) has been used for the detection of hydrogen peroxide [2], cyanide [3], carbon monoxide [4], carbon dioxide [5], phenolic compounds [6] and glucose [7]. Iron (Fe) doping into HA resulted in a strong ferromagnetic material, which found applications in the fields of magnetic resonance imaging, cell separation, drug delivery, and as heat mediators for hyperthermia treatment of cancers and tumor masses [8,9]. Several techniques have been reported to date for the synthesis of iron incorporated nano HA, which includes wet chemical, gel, sol–gel, hydrothermal and microwave methods [10–14]. In this work, we have prepared nano Fe-HA by microwave irradiation method.

L-Tyrosine, one of the amino acids, is indispensable for humans to establish and maintain nutritional balance. Its content in the human body directly reflects the healthy state of people [15,16]. The addition of tyrosine to dietary and food products or pharmaceutical formulations is sometimes necessary due to its limited presence in food material. Tyrosine acts as a precursor for dopa, dopamine, thyroxin, noradrenalin and adrenalin as the hormone or non-tuberculosis mycobacterial (NTM) in mammalian central nervous systems [17]. For instance, tyrosinemia, a congenital metabolic defect, is caused by a deficiency of fumarylacetoacetate hydrolase in the tyrosine degradation pathway. The absence of L-tyrosine could cause hypochondrium, depression and other psychological diseases. However, sister chromatid exchange increases due to a high concentration of L-tyrosine [18,19]. Therefore, the nutritional importance emphasizes the need for reliable analytical methods for the determination of tyrosine in food. Many methods have been applied for the measurement of tyrosine, including fluorometric methods, chemiluminescence, spectrometric analysis, high-performance liquid chromatography and capillary electrophoresis [20–24]. However, most of these methods suffer from some disadvantages, such as high costs, long analysis times and requirement for sample pretreatment. These disadvantages make them unsuitable for routine analysis. Electrochemical methods provide a simple, cost-effective and quick way of analyzing biologically and environmentally important molecules. Unfortunately, the direct electrochemical response of the amino acid at solid electrodes is usually poor. Therefore, chemically modified electrodes are employed to improve the anodic oxidation of amino acids. The most serious drawback of these modified metal electrodes is that they are subject to rapid surface fouling. This problem could be overcome by applying an appropriate enzyme at the electrode surface. Tyrosinase is a copper-containing enzyme protein that catalyzes the oxidation of phenol derivatives, such as tyrosine or tyramine, in the presence of oxygen, to the respective catechol derivatives, e.g., L-dopa or dopamine, which are further oxidized by the enzyme to the respective quinone products [25].

In this work, we have prepared nano Fe-HA by a simple, rapid and efficient microwave irradiation method. These nanoparticles modified glassy carbon electrodes provide a well-defined microenvironment for tyrosinase immobilization and enhanced the direct electron transfer between tyrosinase and electrodes. Interestingly, the electron transfer ability of the nano Fe-HA sample was found to be higher than that of

* Corresponding author. Tel.: +91 9442563637; fax: +91 4565 225202.
E-mail address: Sekar2025@gmail.com (C. Sekar).

0928-4931/$ – see front matter © 2013 Elsevier B.V. All rights reserved.
http://dx.doi.org/10.1016/j.msec.2013.10.013

undoped HA. The constructed biosensor displayed fast electron transfer and a good electrochemical activity for the detection of L-tyrosine with high stability and low detection limit. Therefore, the present work offers a new avenue to broaden the applications of nanostructured Fe-HA in electrochemical biosensors.

2. Experimental procedure

2.1. Preparation of HA and Fe-HA nanoparticles

Calcium hydroxide ($Ca(OH)_2$) and diammonium hydrogen orthophosphate ($(NH_4)_2HPO_4$) were obtained from Merck. Ferric chloride ($FeCl_3$) was purchased from Sisco Research Laboratory, Mumbai and used without further purification. The reaction mixture was prepared by adding a stoichiometric amount of $(NH_4)_2HPO_4$ aqueous solution (0.24 M) to an aqueous suspension of $Ca(OH)_2$ (0.4 M) under constant stirring conditions at room temperature (Eq. 1)

$$10Ca(OH)_2 + 6(NH_4)_2HPO_4 \rightarrow Ca_{10}(PO_4)_6(OH)_2 + 6H_2O + 12NH_4OH \quad (1)$$

The mixture was then exposed to microwave radiation (600 W) for 35 minutes, which resulted in a white powder. This sample was washed with deionized water and dried at 80 °C in a hot air oven. To prepare Fe-doped HA nanoparticles, the above experimental procedure was repeated by mixing $FeCl_3$ (1 M%) with 0.4 M $Ca(OH)_2$. The final product Fe-doped HA was found to be a light-orange powder.

2.2. Electrode preparation and modification

Tyrosinase (TY, T38 1.14.18.1, 3610 units/mg, from mushroom) was purchased from Sigma-Aldrich (St. Louis, MO). A glassy carbon electrode (GCE) was polished with alumina slurry (1.0 and 0.05 μm) and ultrasonically cleaned with 1:1 distilled water and ethanol. The modified electrodes were prepared by a simple drop casting method. The HA nanoparticles were dispersed into doubly-distilled water (5 mg/mL) by sonicating for about 20 min until a homogenous solution was obtained. Typically, 10 μL of HA nanoparticles suspension was mixed with 10 μL of tyrosinase (1 mg/mL, 0.1 M PBS; pH 7.0) solution. Then, 10 μL of the mixed dispersion was cast onto the GC electrode, dried at room temperature (Scheme 1). The electrode was rinsed in 0.1 M phosphate buffer saline (pH 7.0) to eliminate the unadsorbed tyrosinase and stored in pH 7.0 PBS at 4 °C when it was not in use.

2.3. Characterization

Powder X-ray diffraction (XRD) patterns were recorded using a Bruker AXS D8 advanced diffractometer in the 20 range of 20° to 80° (CuKα radiation; λ = 1.5406 Å). Surface morphology and particle size of Fe-HA were characterized by transmission electron microscopy (JEOL 2100 F) with an accelerating voltage of 200 keV. Magnetic measurements were carried out using a Lakeshore VSM 7410 vibrating sample magnetometer (VSM). X-ray photoelectron spectra were recorded at room temperature by using ESCA 3400 apparatus with an Mg Kα (1253.6 eV) X-ray source. All electrochemical measurements were carried out on CHI 608D electrochemical workstation (CH Instruments, Austin, TX) at room temperature. A three-electrode cell was used with a modified glassy carbon electrode (GCE, 3 mm dia) as the working electrode, Ag/AgCl (3 M KCl) as the reference electrode and a platinum wire electrode as the counterelectrode. Cyclic voltammograms (CVs) were recorded between a potential window of −0.2 V and 0.6 V at a scan rate of 50 mV/s in 1 M KCl containing 1.0 mM $[Fe(CN)_6]^{3-/4-}$ redox couple. The electrochemical impedance spectroscopy (EIS) measurements were made by applying AC potential of amplitude 5 mV over the DC potential of 250 mV in the frequency range 100 kHz to 1 Hz. The amperometric measurement was performed in stirred 0.1 M PBS solution of pH 7.0 by applying desired potential to the working electrode and by allowing the steady state current to be reached.

3. Results and Discussion

3.1. Structural analysis

Powder X-ray diffraction (XRD) analysis of nano Fe-HA revealed that the system crystallizes in the hexagonal structure with space group $P6_3/m$ (ICDD card no. 09–0432). The XRD patterns are shown in Fig. 1. Average crystallites size of the products was calculated by using Scherrer's equation (Eq. 2).

$$D = K\lambda/\beta\cos\theta \quad (2)$$

where K is the shape factor (0.9), β is the full-width at half-maximum (fwhm) of diffraction peaks ($h\ k\ l$) measured in radians, λ is the wavelength of the X-rays (λ = 1.5406 Å) and θ is Bragg's diffraction angle. The average crystallite size of undoped HA and Fe-HA were found to be 22.87 and 18.85 nm, respectively. The reduced crystallite size and a small upward shift in peak positions suggest that the dopant Fe^{3+} (ionic radius 0.645 Å) substitutes at the Ca^{2+} (ionic radius 0.99 Å) site in the HA system.

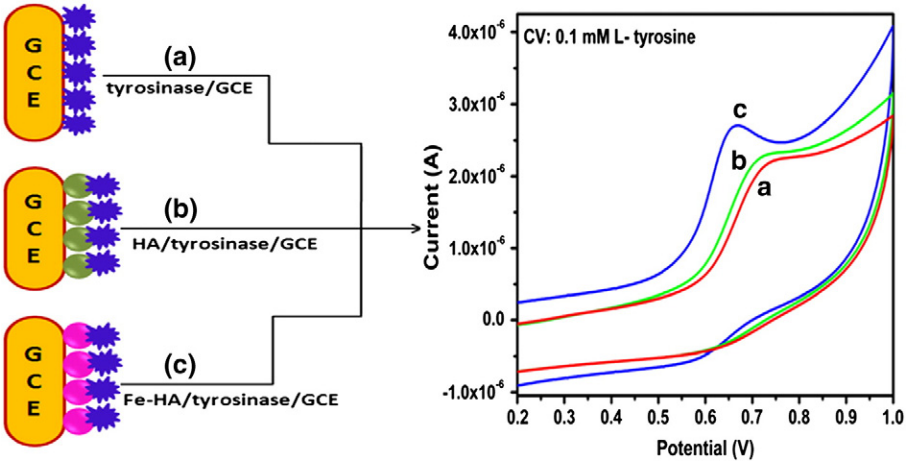

Scheme 1. L-Tyrosine detection scheme using Fe-HA/tyrosinase modified GCE.

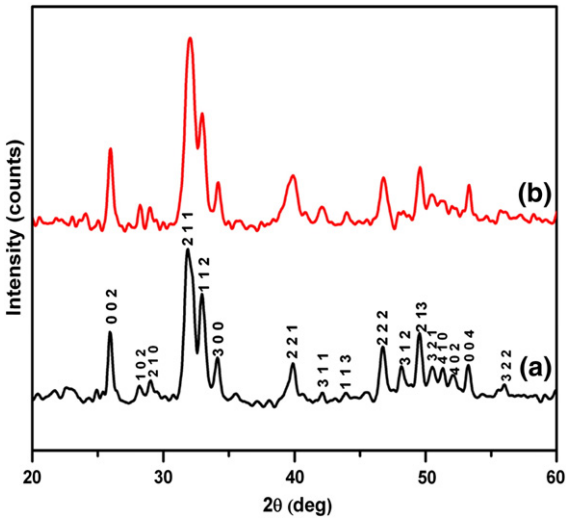

Fig. 1. XRD patterns of HA samples: (a) pure and (b) 1 M% Fe-doped.

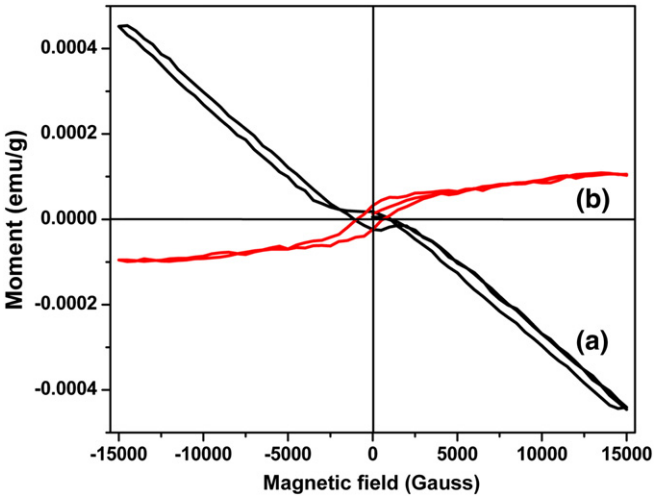

Fig. 3. Magnetization (M) vs. magnetic field (H) curves for (a) pure HA and (b) Fe-doped HA nanoparticles.

3.2. TEM studies of HA

A significant difference in the crystal morphology between the undoped and Fe-doped HA have been observed in the TEM images (Fig. 2). Pristine nano HA have platelet-like shapes with an average particle size of 165 ± 5 nm. On the other hand, Fe-doped HA seemed to form tablet shapes with an average size of 104 (±5) nm. The observed particle size reduction upon Fe doping is in accordance with the XRD results. This type of doping-induced morphological changes and size reductions are desirable for biomedical applications such as biosensor and drug delivery. The investigated undoped HA samples show well-defined lattice fringes without interruption, which is an indication of good crystalline nature. The Fe-doped HA patterns did not indicate the presence of any secondary phase(s). These observations are in good agreement with the XRD results.

3.3. Magnetic studies of HA

To understand the role of ferromagnetic Fe ion impurity on the magnetic characteristics of HA, we have carried out magnetic measurements using vibrating sample magnetometer (VSM). Room temperature magnetization behavior (M–H curves) of pure and Fe-HA samples are shown in Fig. 3. As expected, undoped HA showed diamagnetic behavior and the Fe doping into HA induces ferromagnetism, which is revealed by the appearance of a small hysteresis loop. The magnetization values mainly depend on the charge state of the doped magnetic element. Here, the saturation magnetization (M_S) and retentivity (M_r) values of Fe-HA were found to be 0.11×10^{-3} emu/g and 0.027×10^{-3} emu/g, respectively. This type of induced magnetism in HA is important because it finds applications for targeted drug delivery.

3.4. XPS studies of HA

Fig. 4 shows the X-ray photoelectron spectra (XPS) of the undoped HA and Fe-doped HA nanoparticles. The major peaks found in the XPS spectra are in good agreement with the reported literature [26,27] and were attributed to the chemical state of Ca 2p, P 2p and O 1 s elements in the hydroxyapatite. In general, other metals and impurities were not seen in the spectra recorded between 0 and 1150 eV. The identified peak positions near 348 and 351 eV were attributed to Ca $2p_{3/2}$ and Ca $2p_{1/2}$ respectively. The O1s peaks near 532 eV may be due to oxygen associated with a phosphate group in HA and absorbed water, respectively.

The observed peak positions and their associated reference values are summarized in Table 1. The identified deviations in the binding

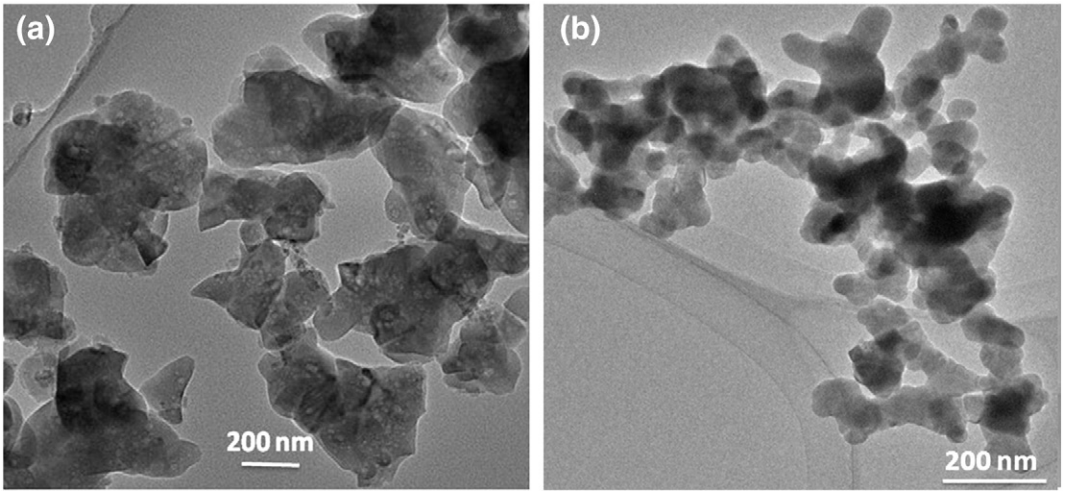

Fig. 2. TEM images of (a) pure HA and (b) Fe-doped HA nanoparticles.

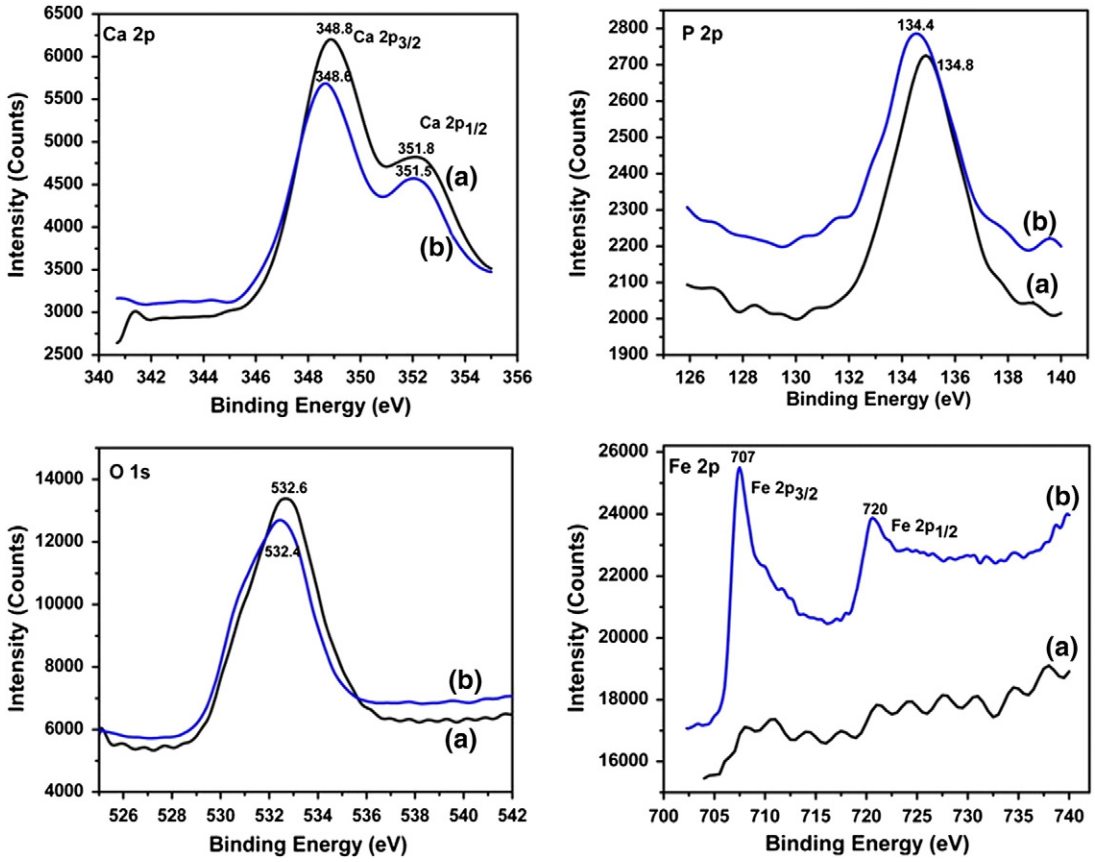

Fig. 4. XPS spectra of (a) pure HA and (b) Fe-doped HA nanoparticles.

energy values corresponding to Ca, P and O elements for undoped and Fe-doped HA confirms the Fe doping into HA and that the constituent elements are in a similar environment in both samples. The binding energies of Fe $2p_{3/2}$ and Fe $2p_{1/2}$ obtained from the present study are 707 and 720.6 eV, respectively. These values lie well within the range of binding energies between 707 and 720 eV reported for Fe $2p_{3/2}$ and Fe $2p_{1/2}$ by many researchers [28,29].

3.5. Electrochemical behavior of HA/tyrosinase-modified electrodes

Electrochemical impedance spectroscopic (EIS) studies have been carried out on all the modified electrodes in the presence of the 1 mM $[Fe(CN)_6]^{3-/4-}$ in 1 M KCl. Fig. 5 shows Nyquist diagrams of electrochemical impedance for fabricated electrodes. The resistance to charge transfer (R_{ct}) values for bare GC (curve a), tyrosinase (curve b), HA/tyrosinase (curve c), and Fe-HA/tyrosinase (curve d) modified electrodes have been estimated as 128, 4319, 2700 and 1973 Ω cm^{-2}, respectively. This means that the electron transfer ability of Fe-HA/tyrosinase > HA/tyrosinase > tyrosinase. The observed results demonstrate that the Fe-HA/tyrosinase can provide a biocompatible microenvironment for tyrosinase and supply a necessary pathway for its direct electron transfer.

Table 1
Binding energies of HA and Fe-HA samples.

Core levels	Measured binding energy (eV)		Literature values for HA (eV) [26,27]
	HA	Fe-HA	
Ca $2p_{1/2}$	351.5	351.8	350.6–350.8
Ca $2p_{3/2}$	348.9	348.7	346.9–347.6
P 2p (PO_4)	134.8	134.4	133.2–134.5
O 1 s	532.7	532.3	530–533

Cyclic voltammograms (CVs) recorded on bare GCE, tyrosinase, HA/tyrosinase and Fe-HA/tyrosinase modified electrodes in the presence of the 1 mM $[Fe(CN)_6]^{3-/4-}$ in 1 M KCl at a scan rate of 50 mV/s are shown Fig. 6A. At bare GCE (curve a), a pair of well-defined redox peak was observed with the peak separation (ΔEp = Epa-Epc) of 70 mV. The tyrosinase (curve b), HA/tyrosinase (curve c) and Fe-HA/tyrosinase (curve d) modified electrodes show the peak separation values (ΔEp) of 256, 163 and 140 mV, respectively. The peak current (i_p) increased and the peak potential separation decreased in the order of bare GC, tyrosinase, HA/tyrosinase, Fe-HA/tyrosinase modified

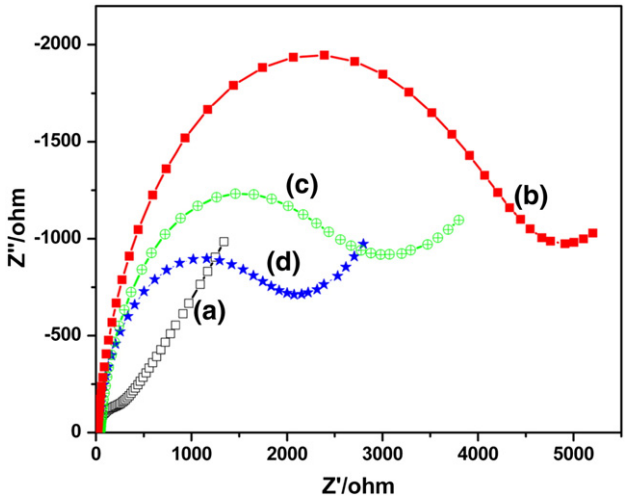

Fig. 5. Electrochemical impedance spectra of (a) bare GCE, (b) tyrosinase, (c) HA/tyrosinase and (d) Fe-HA/tyrosinase modified electrodes recorded in the presence of 1 M KCl solution containing 1 mM $[Fe(CN)6]^{3-/4-}$.

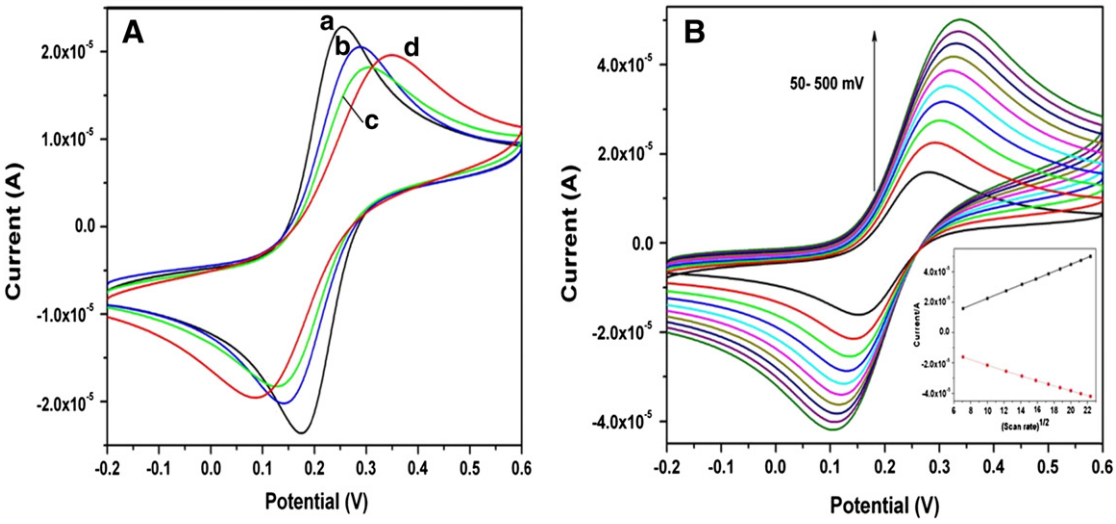

Fig. 6. (A) Cyclic voltammograms of (a) bare GCE, (b) tyrosinase, (c) HA/tyrosinase and (d) Fe-HA/tyrosinase modified GC electrodes in 1 M KCl containing 1 mM $[Fe(CN)6]^{3-/4-}$ recorded at a scan rate of 50 mV/s. (B) Fe-HA/tyrosinase modified GC electrode as a function of scan rate (50–500 mV/s). Inset shows plots of peak current vs. square root of scan rate in 1 M KCl containing 1 mM $[Fe(CN)6]^{3-/4-}$.

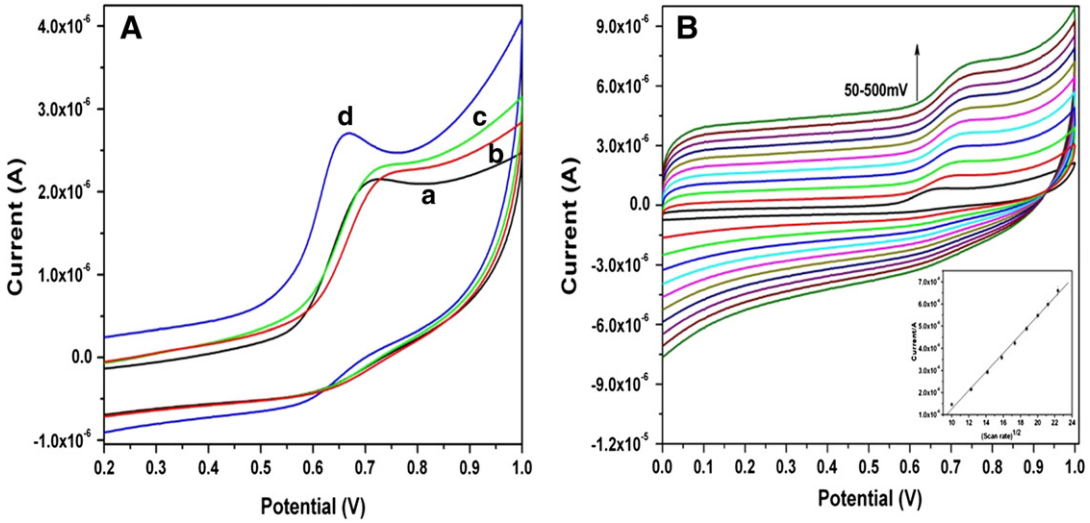

Fig. 7. (A) Cyclic voltammograms recorded at 100 mV/s for (a) bare GCE, (b) tyrosinase, (c) HA/tyrosinase and (d) Fe-HA/tyrosinase modified electrodes in phosphate buffer (0.1 M; pH 7.0) containing 0.1 mM L-tyrosine. (B) CVs obtained for 0.1 mM L-tyrosine at the Fe-HA/tyrosinase modified GC electrode in 0.1 M PBS at different scan rates (50–500 mV/s). Inset shows oxidation current vs. square root of scan rate.

GC electrodes. Based on this CV study, it can be concluded that the Fe-HA/tyrosinase modified GC electrode has a superior electrocatalytic effect towards the catalysis of the ($[Fe(CN)_6]^{3-/4}$) redox reaction. Fig. 6B shows CVs recorded at different scan rates (50–500 mV/s) for Fe-HA/tyrosinase modified electrode in 1 M KCl containing 1 mM of $[Fe(CN)_6]^{3-/4-}$. It can be seen that the anodic potential shifts toward the positive side and the cathodic peak potential shifts in the reverse direction. Besides this, the redox peak currents are proportional to the square root of the scan rate (inset of Fig. 6B), which indicates a diffusion electron-transfer process. To understand the role of Fe concentration in HA nanoparticles, CV and EIS analyses have been performed for pure HA and Fe-doped HA samples (Fe; 1, 5 and 10 M%) in 1 M KCl containing 1 mM $[Fe(CN)_6]^{3-/4}$. The results indicated that the 1 M% Fe-HA modified GC electrode has a superior electrocatalytic effect (Supplementary text and Fig. S1).

3.6. Electrocatalytic oxidation of L-tyrosine

The cyclic voltammograms of a 0.1 mM tyrosine at bare and modified GC electrodes in 0.1 M PB solution (pH 7.0) are shown in Fig. 7A. The oxidation peak current for bare GCE (curve a), tyrosinase (curve b), HA/tyrosinase (curve c) and Fe-HA/tyrosinase (curve d) modified GC electrodes were observed as 2.13×10^{-6} A, 2.22×10^{-6} A, 2.28×10^{-6} A and 2.70×10^{-6} A, and the corresponding oxidation peak potentials were estimated as of 0.71, 0.75, 0.72 and 0.66 V, respectively. The Fe-HA/tyrosinase modified GCE revealed positive potential shift and increased peak current when compared with that of bare GCE, tyrosinase and HA/tyrosinase modified electrodes. The Fe-HA/tyrosinase seem to provide improved electrocatalytic activities and electronic conductivity that in turn effectively catalyzes the L-tyrosine oxidation, which might be ascribed to the enhanced electron transfer of the enzymatic reaction shown in Eq. (3) in the presence of Fe-HA. The high permeability of Fe-HA film seems to help electrolytes to penetrate through the film and to gain access to the interior surface more easily. Hence, we have used Fe-HA/tyrosinase modified electrodes for further investigation.

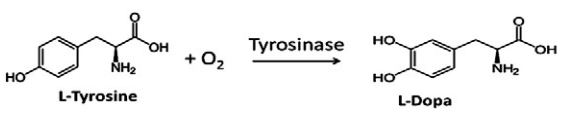

(3)

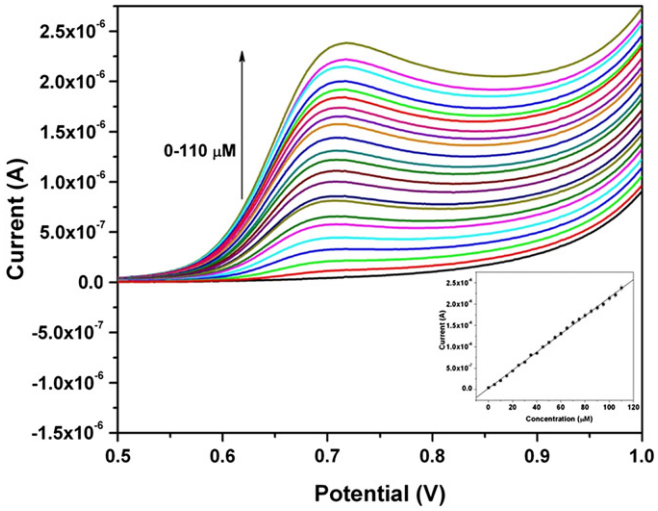

Fig. 8. LSVs obtained for L-tyrosine in the concentrations ranging from 0 to 110 μM. L-Tyrosine was added in steps of 5 μM each at the Fe-HA/tyrosinase modified GC electrode in PB solution (pH 7.0) at a scan rate of 50 mV/s. Inset shows the calibration plot.

Fig. 7B shows the CVs of Fe-HA/tyrosinase modified electrode recorded with different scan rates (50–500 mV/s) in 0.1 M PB solution (pH 7.0) containing 0.1 mM of L-tyrosine. The oxidation peak heights were found to increase linearly with the square root of scan rate from 50 to 500 mV/s. The regression equation was deduced as I_{pa} (μA) = 0.420 (Vs^{-1}) + 2.943, $r = 0.998$ (inset of Fig. 7B). These results confirmed that the electrode reaction of L-tyrosine was under diffusion control.

Fig. 8 shows the linear sweep voltammograms (LSVs) obtained for L-tyrosine in the concentration range of 10 to 100 μM at the Fe-HA/tyrosinase modified electrode. The oxidation current of L-tyrosine was increased with a slight negative potential shift in the oxidation peak potential upon each increment of 5 μM. The oxidation currents had a linear relationship with the concentration of L-tyrosine with a correlation coefficient of 0.999 (inset of Fig. 8).

3.7. Amperometric determination of L-tyrosine

The amperometric response of the Fe-HA/tyrosinase modified electrode to L-tyrosine was investigated by successive additions of standard L-tyrosine solution to a continuous stirring electrolyte solution in an electrochemical cell under a physiological pH of 7.0 in 0.1 M PBS at an applied potential of 0.66 V. Fig. 9A shows typical current–time (*i*–*t*) responses for the successive additions of L-tyrosine. The Fe-HA/tyrosinase modified electrode shows the initial current response due to 500 nM of L-dopa in each step with a sample interval of 50 s, the current response increases and a steady state current response was attained within 5 s. Furthermore, the amperometric current response increased linearly with increasing L-tyrosine concentration in the range of 1.0×10^{-7} to 1.1×10^{-5} M with a correlation coefficient of 0.999 (inset of Fig. 9A) and the detection limit was found to be 245 nM. The efficiency of the present sensor was compared with the other L-tyrosine sensors reported in the literature (Table 2).

To evaluate the selectivity of the L-tyrosine sensor, many interferents such as urea, sucrose, galactose, boric acid and oxalic acid were investigated. Fig. 9B shows the amperometric *i*–*t* curve obtained for L-tyrosine at Fe-HA/tyrosinase modified electrode in the presence of several interferents in a homogeneously stirred 0.1 M PB solution (pH 7.0). The amperometric responses of the biosensor towards the additions of 100 μM of L-tyrosine (a) and 10 mM each (b) boric acid, (c) oxalic acid, (d) urea, (e) galactose and (e) sucrose separately with a sample interval of 50 s to the same solution. No change in current response was observed due to the addition of the interferent compounds. These results indicate that the determination of 100 μM of L-tyrosine is possible even in the presence of 100-fold excess of common interferents, which suggests a high selectivity and favorable ability of anti-interference towards the determination of L-tyrosine on Fe-HA/tyrosinase/GCE. In addition, the influence of other possible interfering species such as Mg^{2+}, Ca^{2+}, Na^{+}, K^{+} and lactase has been investigated and no interference effect was observed (Supplementary Fig. S2).

3.8. Reproducibility and selectivity of the developed biosensor

The reproducibility of the Fe-HA/tyrosinase modified electrode has been evaluated by comparing the response currents of five electrodes. The relative standard deviation (RSD) was 4.20% in 1.0 mM of L-tyrosine. The operational stability was examined continuously for 10 times for the same electrodes, and the RSD of the response current was found to be 5.7%. The long-time stability of the fabricated electrodes was tested in a phosphate buffer solution (pH 7.0, 4 °C) after 2 weeks. The response current retained 80% of the initial value, which indicates that the Fe-HA/tyrosinase film is very stable and that the matrix can prevent enzyme from leaking, contamination and biodegradation.

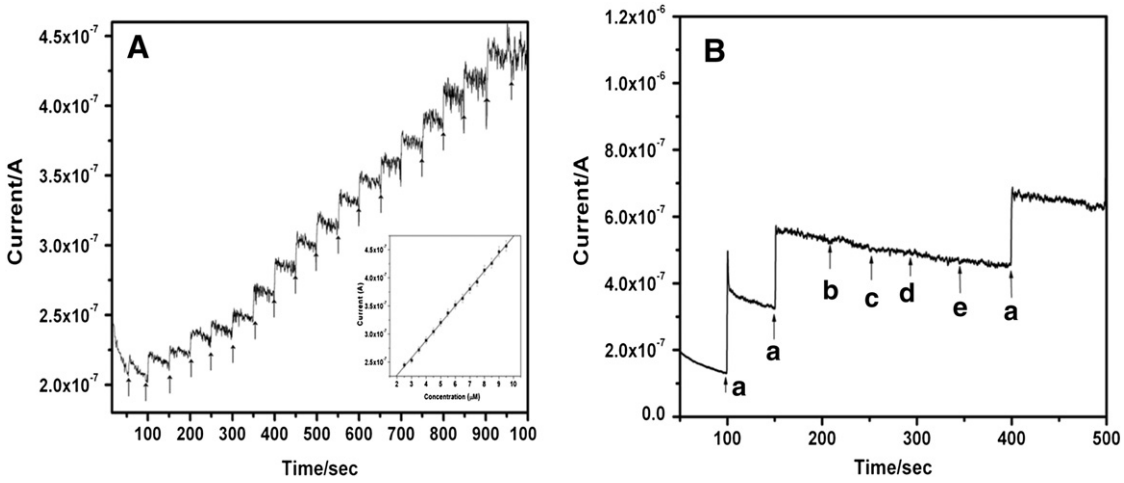

Fig. 9. (A) Amperometric (*i*–*t*) response for the successive additions of 500 nM of L-tyrosine at Fe-HA/tyrosinase modified electrode in 0.1 M PB solution (pH 7.0) with the applied potential of 0.66 V (arrows indicate the L-tyrosine injection). Inset shows the calibration plot. (B) Amperometric response for the addition of (a) 100 μM L-tyrosine in the presence of various interferents such as 10 mM each (b) boric acid, (c) oxalic acid, (d) urea, (e) galactose and (e) sucrose at Fe-HA/tyrosinase modified GCE in 0.1 M PB solution (pH 7.0) with an applied potential of 0.66 V. The noise is due to stirring the analyte solution.

Table 2
Comparison of proposed L-tyrosine biosensor with others.

Electrode	pH	Linear range (M)	Detection limit (M)	References
MWCNT/4-amino benzene sulfonic acid, GCE	7.0	1×10^{-7} to 5×10^{-5}	8×10^{-8}	[30]
MWCNT, GCE	6.5	9×10^{-7} to 3.5×10^{-4}	3.5×10^{-7}	[31]
MWCNT, ionic liquid, copper (II), GCE	5.5	1×10^{-8} to 5×10^{-6}	8×10^{-9}	[32]
Polypyrrole, Ni electrode MIP	2.0	5×10^{-3} to 4.5×10^{-2}	–	[33]
Cu(II), HMDE	9.6	1×10^{-7} to 5×10^{-5}	5×10^{-8}	[34]
Zeolite, carbon paste	3.0	1.26×10^{-6} to 9×10^{-5}	3.2×10^{-7}	[35]
Boron-doped diamond electrode	11.2	2×10^{-5} to 1×10^{-3}	1×10^{-6}	[36]
MWCNT, GCE	7.0	2×10^{-6} to 5×10^{-4}	4×10^{-7}	[37]
Gold nanoparticles, GCE	7.0	1×10^{-7} to 3×10^{-4}	4×10^{-8}	[38]
Copper (II), MICP, MIP	5.5	1×10^{-8} to 1×10^{-6}	4×10^{-9}	[39]
*Fe-HA/tyrosinase	7.0	1.0×10^{-7} to 1.1×10^{-5}	2.45×10^{-7}	Present work

* Hydroxyapatite is highly biocompatible.

The main advantage of the fabricated sensor is that the sensing material (nano Fe-HA) is biologically compatible and that it can be prepared by a simple microwave irradiation method. Furthermore, the electrode modification was done by a simple drop cast method. The doping-induced lattice strain of Fe-HA seemed to provide a suitable microenvironment, large amounts of enzyme loading and enhanced direct electron transfer between the enzyme's active sites and the electrode. Moreover, Fe-HA modified electrode exhibits electric conductivity and electrochemical activity in neutral pH (7.0) solutions, which can be used for the entrapment of a wide range of biomolecules.

4. Conclusion

We have fabricated a novel L-tyrosine biosensor based on Fe-HA/tyrosinase modified glassy carbon electrode in neutral pH (7.0). The bioinorganic Fe-HA nanoparticle enabled improved electron transfer between tyrosinase and Fe-HA modified electrode surfaces. The amperometric current has a wide linear dynamic range of 1.0×10^{-7} to 1×10^{-5} M and the lower detection limit was found to be 245 nM. The Fe-HA modified electrode was found to be sensitive and selective towards the determination of L-tyrosine in the presence of 100-fold boric acid, oxalic acid, urea, galactose and sucrose. The fabricated biosensor exhibited high reproducibility, long-term stability and satisfactory anti-interference ability. These results demonstrate that the nanostructured Fe-doped hydroxyapatite is an attractive material for the fabrication of efficient amperometric biosensors.

Acknowledgements

One of the authors (P.K.) acknowledges with thanks the Council of Scientific and Industrial Research (CSIR), Government of India for providing the Research Associateship (F.No. 9/688(0022)/12 EMR-I). C.S. acknowledges the CSIR for funding (F.No. 03 (1203)/12/EMR-II). The authors thank Prof. Y. Hayakawa, Dr. M. Navaneethan and Dr. M. Arivanadhan of Research Institute of Electronics, Shizuoka University, Japan and S. Radhakrishnan, Department of Bioelectronics and Biosensors, Alagappa University, for their help in experimental work.

Appendix A. Supplementary data

Supplementary data to this article can be found online at http://dx.doi.org/10.1016/j.msec.2013.10.013.

References

[1] Y. Yuan, S.L. Tang, H. Hong, C.S. Liu, Chin. J. Biomed. Eng. 24 (2005) 27–30.
[2] B. Wang, J.J. Zhang, Z.Y. Pan, X.Q. Tao, H.S. Wang, Biosens. Bioelectron. 24 (2009) 1141–1145.
[3] S. Wang, Y. Lei, Y. Zhang, J. Tang, G. Shen, R. Yu, Anal. Biochem. 398 (2010) 191–197.
[4] R.U. Mene, M.P. Mahabole, R. Sharma, R.S. Khairnar, Vacuum 86 (2011) 66–71.
[5] R.U. Mene, M.P. Mahabole, R. Sharma, R.S. Khairnar, Radiat. Phys. Chem. 80 (2011) 682–687.
[6] L. Lu, L. Zhang, X. Zhang, S. Huan, G. Shen, R. Yu, Anal. Chim. Acta. 665 (2010) 146–151.
[7] Q. Zhang, C. Chen, Q. Xie, P. Liu, Microchim. Acta 165 (2009) 223–229.
[8] Z. Stojanovic, L. Veselinovic, S. Markovic, N. Ignjatovic, D. Uskokovic, Mater. Manuf. Process. 24 (2009) 1096–1103.
[9] S.F. Kabir, S. Ahmed, A.I. Mustafa, M. Ahsan, S. Islam, Bangladesh J. Sci. Ind. Res. 47 (2012) 1–8.
[10] M.R. Saeri, A. Afshar, M. Ghorbani, N. Ehsani, C.C. Sorrell, Mater. Lett. 57 (2003) 4064–4069.
[11] P. Kanchana, C. Sekar, J. Cryst. Growth 312 (2010) 808–816.
[12] C.M. Mardziah, I. Sopyan, S. Ramesh, Trends Biomater. Artif. Organs 23 (2009) 105–113.
[13] M.O. Li, X. Xiao, R. Liu, C. Chen, L.J. Huang, J. Mater. Sci. Mater. Med. 19 (2008) 797–803.
[14] W. Pon-On, S. Meejo, Int. J. Nanosci. 6 (2007) 9–16.
[15] A. Carlsson, M. Lindqvist, N.S. Arch, Pharmacology 303 (1978) 157–164.
[16] J.P. Jin, X.Q. Lin, Electrochem. Commun. 6 (2004) 454–460.
[17] G. Beck, C. Hanusch, P. Brinkkoetter, N. Rafat, J. Schulte, K. Ackern, B. Yard, Anaesthesist 54 (2005) 1012–1020.
[18] O.Y. Al-Dirbashi, M. Jacob, L.Y. Al-Ahaidib, K. Al-Qahoni, Z. Rahbeeni, M. Al-Owain, M.S. Rashed, Clin. Chim. Acta 365 (2006) 243–248.
[19] C.Y. Li, Colloids Surf. B 50 (2006) 147–151.
[20] F. Wang, K.Z. Wu, Y. Qing, Y.X. Ci, Anal. Lett. 25 (1992) 1469–1478.
[21] S. Alonso, L. Zamora, M. Calatayud, Talanta 60 (2003) 369–376.
[22] C.J. Lee, J. Yang, Anal. Biochem. 359 (2006) 124–131.
[23] Y. Ishii, M. Iijima, T. Umemura, A. Nishikawa, Y. Iwasaki, R. Ito, K. Saito, M. Hirose, H. Nakazawa, J. Pharm. Biomed. Anal. 41 (2006) 1325–1331.
[24] Y. Huang, X.Y. Jiang, W. Wang, J.P. Duan, G. Chen, Talanta 70 (2006) 1157–1163.
[25] H.B. Yildiz, R. Freeman, R. Gill, I. Willner, Anal. Chem. 80 (2008) 2811–2816.
[26] S. Kaciulis, G. Mattogno, L. Pandolfi, M. Cavalli, G. Gnappi, A. Montenero, Appl. Surf. Sci. 151 (1999) 1–5.
[27] M.C. Changa, J. Tanaka, Biomaterials 23 (2002) 3879–3885.
[28] A.P. Grosvenor, B.A. Kobe, M.C. Biesinger, N.S. McIntyre, Surf. Interface Anal. 36 (2004) 1564–1574.
[29] T. Yamashita, P. Hayes, Appl. Surf. Sci. 254 (2008) 2441–2449.
[30] K. Huang, D. Luo, W. Xie, Y. Yu, Colloids Surf. B 61 (2008) 176–181.
[31] J. Xu, Y. Wang, Y. Xian, L. Jin, K. Tanaka, Talanta 60 (2003) 1123–1130.
[32] L. Liu, F. Zhao, F. Xio, B. Zeng, Electroanalysis 20 (2008) 2148–2152.
[33] H. Liang, T. Ling, J.F. Rick, T. Chou, Anal. Chim. Acta. 542 (2005) 83–89.
[34] L. Wang, C. Ma, X. Zang, Y. Ren, Y. Yu, Fresenius J. Anal. Chem. 351 (1995) 689–691.
[35] A. Babaei, S. Mirzakhani, B. Khalilzadeh, J. Braz. Chem. Soc. 20 (2009) 1862–1869.
[36] G. Zhao, Y. Qi, Y. Tian, Electroanalysis 18 (2006) 830–834.
[37] Q. Xu, S. Wang, Microchim. Acta 151 (2005) 47–52.
[38] Z. Chen, K. Okamura, M. Hanaki, T. Nagaoka, Anal. Sci. 18 (2002) 427–432.
[39] Varghese Saumya, Krishnapillai P. Prathish, Talasila P. Rao, Talanta 85 (2011) 1056–1062.